ELSEVIER

Biochimica et Biophysica Acta 1283 (1996) 111–118

BBA Biochimica et Biophysica Acta

Interdigitation of bilayers from ether lipid analogs: (*R*)-PAF, (*R*)-Lyso-PAF and the antineoplastic (*R*)-ET-18-OMe

Xiangqun Xie [a], Sonyuan Lin [b], Jill Moring [b], Alexandros Makriyannis [a,b,*]

[a] *Institute of Materials Science, University of Connecticut, Storrs, CT 06269, USA*

[b] *Department of Pharmaceutical Sciences, School of Pharmacy, University of Connecticut, Storrs, CT 06269, USA*

Received 30 October 1995; revised 7 March 1996; accepted 9 April 1996

Abstract

The ether lipid analogs (*R*)-PAF, (*R*)-ET-18-OMe and (*R*)-Lyso-PAF can form bilayers. Using differential scanning calorimetry (DSC) and small angle X-ray diffraction, we have investigated bilayers formed entirely of these molecules. Small angle X-ray diffraction experiments strongly indicated that these bilayers are interdigitated at 98% relative humidity in the gel phase. The slight differences in the structures of the ether lipids affect their thermal behavior and packing properties. Of the three, (*R*)-Lyso-PAF shows the highest phase transition temperature, broadest phase transition peak and smallest enthalpy change. These characteristics may be attributed to hydrogen bonding of the -OH group at *sn*-2 position of its glycerol backbone to water or to other (*R*)-Lyso-PAF molecules. The interdigitated structure shows that these bilayers are similar to lipid bilayers and suggests that these molecules could easily insert themselves into membranes to reach their respective active sites or to perturb the membranes. The packing and thermal characteristics of (*R*)-Lyso-PAF may help explain its biological inactivity.

Keywords: Ether lipid; Platelet activating factor; Antineoplastic agent; X-ray diffraction; Small-angle X-ray diffraction; DSC

1. Introduction

Ether lipids have several important biological activities [1–5]. Platelet activating factor (1-*O*-alkyl-2-acetyl-*sn*-glycero-3-phosphocholine) (PAF) directly or indirectly affects an astonishing range of physiological processes in a wide variety of tissues, and acts as a mediator in several disease states [6–8]. PAF is also structurally diverse. The *sn*-1 chains may vary in length, may be saturated or unsaturated, and may have either an ether or ester linkage [9]. One ether lipid analog investigated in this work, (*R*)-1-*O*-octadecyl-2-*O*-acetyl-*sn*-glycero-3-phosphocholine [(*R*)-PAF] (Fig. 1), acts as a platelet activating factor [10]. Another, (*R*)-1-*O*-octadecyl-2-*O*-methyl-*sn*-glycero-3-phosphocholine [(*R*)-ET-18-OMe], not only has antineoplastic activity [11,12] but is also a member of a new class of membrane-active anti-HIV agents [13]. Yet, the closely related ether lipid analog (*R*)-Lyso-PAF, in which the -OMe group of (*R*)-ET-18-OMe or the acetyl group of (*R*)-PAF has been replaced by -OH (Fig. 1), has no similar biological activities. Understanding of the structure–function relationships of these substances [3,4] can be increased by a detailed study of the specific interaction principles, packing properties and thermal behavior of these molecules.

This work is focused on membranes composed of each ether lipid alone, with no model membranes present. Study of these simple systems permits insight into the interactions of these molecules with one another and with water that crystal structures and studies of these molecules in model membranes cannot provide. Our experiments show that all three compounds can form bilayers.

Huang et al. have conducted extensive empirical studies of interdigitated gel phases in fully hydrated phosphatidylcholines. They have predicted the existence of these phases from the difference in length of the two hydrocarbon chains, even predicting the temperature of the phase transition [14,15]. Although their studies were conducted using acyl rather than ether lipids, a broad application of their work predicts the existence of an interdigitated lamellar gel phase for these three compounds. The present work confirms the existence of this phase and provides detailed information on its structure for these three compounds. In

* Corresponding author: School of Pharmacy U-92, University of Connecticut, 372 Fairfield Road, Storrs, CT 06269-2092, USA. Fax: +1 (860) 4863089; e-mail: makriyan@uconnvm.uconn.edu.

PII S0005-2736(96)00085-5

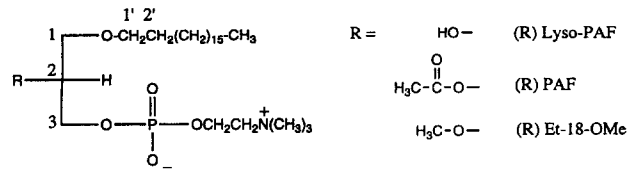

Fig. 1. Chemical structures of the ether lipid analogs.

small-angle X-ray diffraction experiments these molecules gave electron density profiles typical of interdigitated bilayers, with *d*-spacings of about 42 to 50 Å in the gel phase at 98% relative humidity (RH). The DSC data confirm these results and show that the gel-liquid crystalline phase transitions of these molecules at 98% RH occur at 25–30°C.

2. Materials and methods

2.1. Synthesis

(*R*)-PAF, (*R*)-ET-18-OMe and (*R*)-1-*O*-octadecyl-*sn*-glycero-3-phosphocholine [(*R*)-Lyso-PAF] (Fig. 1) were synthesized in our laboratories using modifications of published synthetic methods [12,16,17]. 2,3-*O*-Isopropylidene-1-*O*-octadecyl-*sn*-glycerol was prepared by the method of Hirth and Barner [16]. Alternatively, 2,3-*O*-isopropylidene-*sn*-glycerol was refluxed with KOH and 1-bromooctadecane in toluene [2]. The isopropylidene moiety was replaced by the benzylidene group by refluxing with benzylaldehyde in the presence of catalytic *p*-toluenesulfonic acid for 5 h [18]. The resulting 2,3-*O*-benzylidene-1-*O*-octadecyl-*sn*-glycerol was a 45:55 (*cis* to *trans*) mixture of epimers at the benzylidene carbon. Reductive opening of the benzylidene was carried out by using a solution of $LiAlH_4$ and $AlCl_3$ in Et_2O, giving a 4:1 mixture of 3-*O*-benzyl-1-*O*-octadecyl-*sn*-glycerol and 2-*O*-benzyl-1-*O*-octadecyl-*sn*-glycerol. The minor product was then treated with β-bromoethyldichlorophosphate [19–21]. Trimethylamine was used to give (*R*)-2-*O*-benzyl-1-*O*-octadecyl-*sn*-glycero-3-phosphocholine. This was debenzylated by hydrogenolysis using palladium hydroxide as a catalyst to give 1-*O*-octadecyl-*sn*-glycero-3-phosphocholine [(*R*)-Lyso-PAF]. This was acetylated using acetic anhydride in $CHCl_3$ to give 2-*O*-acetyl-1-*O*-octadecyl-*sn*-glycero-3-phosphocholine [(*R*)-PAF] [22].

(*R*)-2-*O*-methyl-1-*O*-octadecylglycero-3-phosphocholine [(*R*)-ET-18-OMe] was synthesized by the method reported for the preparation of 1-*O*-alkyl-2-*O*-alkyl′-*sn*-glycerols [12,23] starting with 2,3-*O*-isopropylidene-*sn*-glycerol via β-bromoethyl phosphodiesters [19–21].

The optical purities of the *sn*-glycero-3-phosphocholine ether lipids as percent enantiomeric excess (% ee) were determined unambiguously by ^{1}H-NMR after converting a synthetic precursor to its (*R*)-3,3,3-trifluoro-2-methoxy-2-phenylpropionate (Mosher's ester) [24]. The optical purity of the 1-*O*-alkyl-3-benzyl-*sn*-glycerol (prepared from 2,3-*O*-isopropylidene-*sn*-glycerol) was found to be 99.0 ± 0.5% ee from the integration of the benzyl protons in the ^{1}H-NMR spectra of the corresponding Mosher's ester [23]. The (*R*)-isomer of each compound was used exclusively in all of our experiments.

2.2. Small-angle X-ray diffraction

Partially hydrated (≈ 98% RH) vesicle dispersions were prepared by first drying 1 mg of the compounds in test tubes under vacuum for 12 h to remove residual organic solvents. Then ≈ 1 ml distilled water was added while the samples were being vortexed. The resulting suspensions were sonicated in a bath sonicator for 15 min until the suspension became translucent. After sonication, ≈ 15 μl of the vesicle suspension was pipetted onto aluminum foil and dried at ≤ 35°C. The pipetting and drying were repeated twice more; then the samples were mounted on a curved glass support. The samples were partially rehydrated for 24 h in closed vials over a saturated solution of sodium sulfate to maintain ≈ 98% RH, then sealed in brass diffraction canisters containing potassium sulfate solution. Occasionally, especially for the purpose of phase determination, data were collected at partial hydration states other than that resulting from 98% RH. 98% RH provides a high hydration state, but not full hydration. The result of partial hydration is better sample order and thus better X-ray diffraction, while reasonable physiological relevance is maintained.

Diffraction data were collected using an Elliot GX18 rotating anode microfocus generator (Marconi Avionics) supplying Cu K_α radiation ($\lambda = 1.54$ Å) in conjunction with a fixed-geometry beamline consisting of a single Franks mirror providing line focus at the detection plane, vertical and horizontal limiting slits, a nickel filter, the curved specimen, a tungsten beamstop, and electronic detection. The beam height at the specimen was ≈ 1 mm. Small angle X-ray diffraction patterns were collected using a Braun one-dimensional position-sensitive proportional counting gas flow detector (Innovative Technology, South Hamilton, MA). The specimen-to-detector distance was 130 mm. Most data were collected at 14°C; some were collected at higher temperatures. Data were transferred directly to a VAX computer system for reduction and analysis. Phases were determined by a swelling series [25,26]. It was assumed that the electron density profiles should be consistent with a bilayer structure. Repetitions of the diffraction experiments for each compound at 98% RH gave electron density profiles consistent with those from the original experiments.

2.3. Differential scanning calorimetry

DSC experiments at 98% RH were carried out to investigate the mesomorphic properties of the preparations and

to help interpret the diffraction data. Partially hydrated vesicle samples were made using the same method as for the X-ray samples, but with 5 mg of compound. The vesicle samples were deposited on a glass surface, dried, and scraped into stainless steel DSC pans (Perkin Elmer, 0.25 cm height × 0.5 cm diameter). The sample pans were suspended in closed vials at 98% RH for 48 h, then sealed. After the pans were sealed, several cycles of heating the sample above its transition temperature and then cooling were carried out to assure proper mixing. Sometimes the samples were cycled through the phase transition at 98% RH several times both before and after sealing the pans, to assure that the hydration state was as homogeneous as possible at 98% RH. This process did not alter the shape of the transition. The DSC experiments were conducted in a Perkin Elmer DSC-7 instrument at a scan rate of 2.5 K/min over a suitable temperature range for each compound.

2.4. Computer graphic representation

Molecular modeling and graphic display were performed on a 4D/70GT IRIS Silicon Graphics workstation using the Biosym InsightII(2.2.0)/Discover(2.9.0) molecular modeling package (Biosym, San Diego, CA). The structures of the individual alkyl lysophospholipid molecules were built from the X-ray crystallographic model of (*R*)-ET-18-OMe [27] and were energy-minimized using the Biosym program. The minimum energy conformation of (*R*)-ET-18-OMe was then used as a starting template on which the structures of (*R*)-PAF and (*R*)-Lyso-PAF were generated by deletion and/or addition of atoms at standard bond lengths and bond angles under the Biosym software. The energy-minimized molecules were used to build bilayer structures consistent with the experimental electron density profiles.

3. Results

3.1. Small angle X-ray diffraction

Fig. 2 shows a typical set of diffraction data from (*R*)-ET-18-OMe. The quality of the data from the other ether lipids was similar. Swelling experiments were conducted to determine the phases [25,26]. The phases were deduced by observation of the behavior of the transform close to the nodes and by use of the minimum wavelength principle [28]. Fig. 3 shows the structure factors for (*R*)-PAF, (*R*)-ET-18-OMe and (*R*)-Lyso-PAF. The bilayers showed only small structural changes, which were interpreted as the effect of increased disorder of the ether lipid molecules at higher water contents.

The reflections between 0.00 Å^{-1} and 0.10 Å^{-1} were

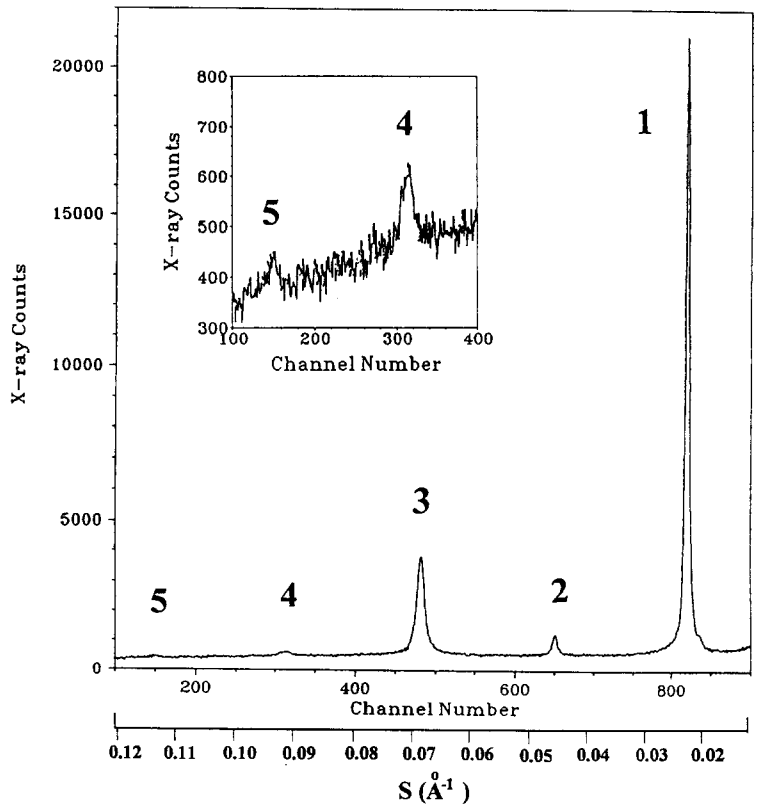

Fig. 2. A diffraction pattern from (*R*)-ET-18-OMe at 98% RH and 14°C, before Lorentz and background correction. The inset shows the fourth and fifth orders, scaled up. Diffraction quality from (*R*)-PAF and (*R*)-Lyso-PAF was similar.

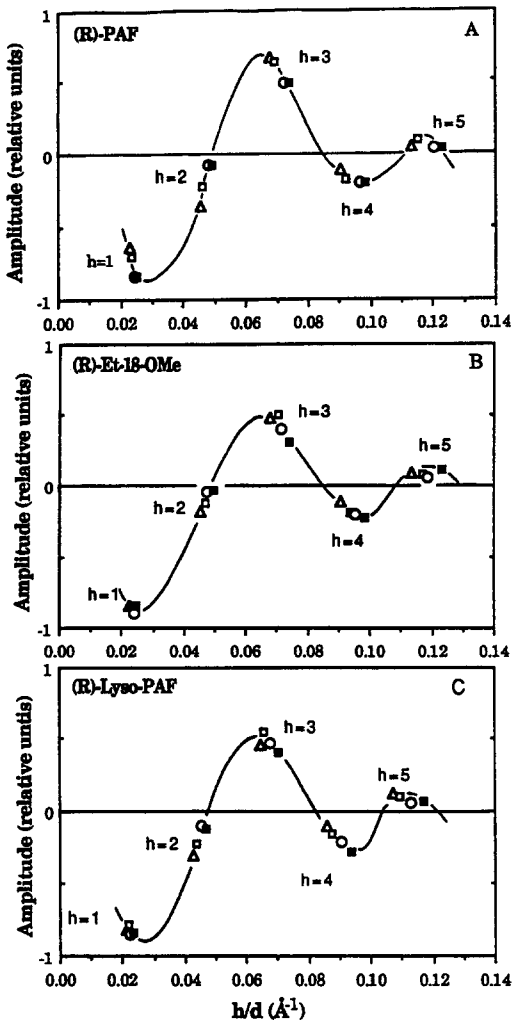

Fig. 3. Structure factors [diffraction amplitude vs. h/d (Å^{-1})] of the three ether lipid analogs. Samples were equilibrated at 98% RH (△), 87% RH (□), 66% RH (○), and 13% RH (■) at 14°C.

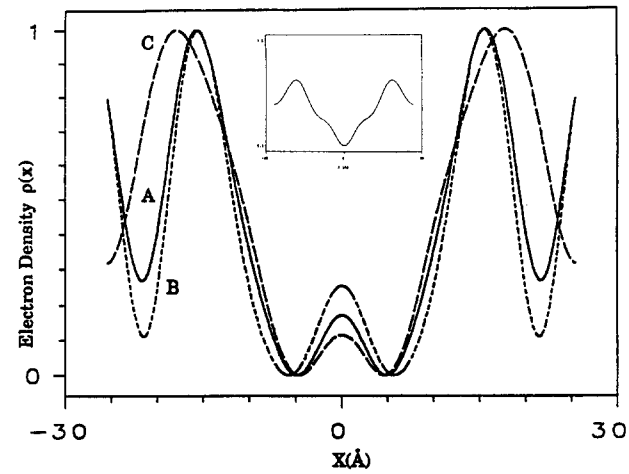

Fig. 4. Electron density profiles of the three ether lipid analogs at 98% RH and 14°C, showing the typical pattern of interdigitated bilayers. A, (*R*)-PAF, $d = 43.30$ Å; B, (*R*)-ET-18-OMe, $d = 42.93$ Å; C, (*R*)-Lyso-PAF, $d = 50.96$ Å. The profiles have been normalized to 1 because there is no absolute electron density scale; the electron density is in arbitrary units. Superimposition of the electron density profiles shows differences at the center interdigitated regions of the terminal alkyl chains and in the water regions (see text). The inset shows an electron density profile of DMPC at 12°C (in the gel state, not interdigitated) for comparison.

easily assigned phases, but because of the extended zero in the data at about 0.12 Å^{-1}, the phases in that region were ambiguous. These reflections could be given phases of either 0 or π without violating the minimum wavelength principle. Therefore, we assumed that the electron density profiles should be consistent with a bilayer structure. All phase combinations were systematically tested for each set of data, and only one combination in each case gave a profile that was consistent with a bilayer structure. The structure factors for the three molecules fell on similar smooth curves, which provided evidence that all of the ether lipids had the same phases (π,π,0,π,0) for the structure factors corresponding to the 1st, 2nd, 3rd, 4th, and 5th orders.

Using the correct phase combination, we calculated electron density profiles (Fig. 4) for (*R*)-PAF, (*R*)-ET-18-OMe and (*R*)-Lyso PAF at 98% RH and 14°C (in the gel phase). In each profile the two peaks representing the lipid headgroups were centered at approximately ±17 Å. The intermediate-density regions at the edges of the profile, outside the headgroup peaks, represent the water spaces between the bilayers. The central low-density region between the headgroup peaks, which represents the hydrocarbon core, contained two lowest-density regions separated by about 10 Å. In contrast, a typical dimyristoylphosphatidylcholine (DMPC) electron density profile has a single central trough in this region, representing the methyl groups (inset, Fig. 4). The presence of the small peak in the center of the profile suggests that in these ether lipids, hydrocarbon chains from opposing monolayers have interpenetrated.

The electron density profiles in Fig. 4 were normalized so that the headgroups and lowest density regions of all of the profiles fall at 1.0 and 0.0 on the scale, respectively. The absence of an absolute electron density scale prohibits direct comparison of electron densities among the three structures, but electron densities *within* each individual profile can be compared, as well as the overall shapes of the profiles. The major differences in the profiles for the three occur in the central low-density region between the headgroup peaks, that is, in the hydrocarbon core of the bilayer. Related differences occur in the water space. (*R*)-Lyso-PAF has the lowest electron density at the central region (compared to the density of its *own* headgroup region, *not* to the central regions of the other two structures or to their headgroup regions), and the highest electron density at the water space between the headgroups from two adjacent bilayers. (*R*)-ET-18-OMe has the highest relative electron density at the bilayer center and the lowest in the water space. (*R*)-PAF has intermediate rela-

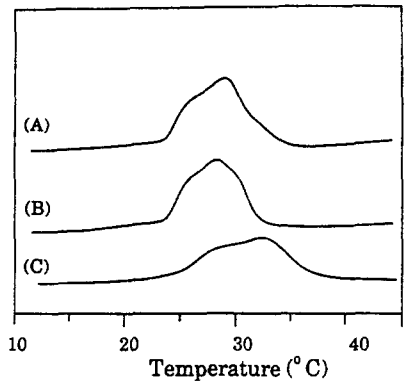

Fig. 5. DSC scans showing the main transition of (*R*)-PAF (A), (*R*)-ET-18-OMe (B), and (*R*)-Lyso-PAF (C), rehydrated at 98% RH to be analogous to the X-ray samples. The heating rate was 2.5 K/min. The scans were normalized to enthalpy per gram because of slightly different masses of the ether lipids in the samples.

tive values in both regions. This suggests a relationship between the degree of interdigitation of the chains and the amount of water incorporated between the bilayers. The electron density between bilayers for (*R*)-ET-18-OMe is less than that at the bilayer center. Its headgroup peak is relatively narrow, and its interdigitated region is relatively wide. These characteristics indicate that its lipid packing is probably the most efficient of the three. The broad headgroup peak of (*R*)-Lyso-PAF suggests that its -OH group may attract more water through H-bonding than the *sn*-2 substituents of (*R*)-ET-18-OMe or (*R*)-PAF do, causing less efficient lipid packing and spreading out the headgroup electron density.

3.2. Differential scanning calorimetry

Fig. 5 shows the main phase transitions of (*R*)-PAF, (*R*)-ET-18-OMe, and (*R*)-Lyso-PAF at 98% RH. All three molecules gave broad phase transition peaks with a shoulder at the low-temperature side. The shoulder indicates either that two populations are involved in the transition, or that two transitions are taking place. Two populations might correspond to two hydration states due to inhomogeneous hydration at 98% RH. Accordingly, some samples were annealed by cycling several times through the phase transition at 98% RH before the pans were sealed, as well as after sealing, to ensure that hydration was homogeneous. This procedure did not change the shape of the endotherms. (*R*)-Lyso-PAF gave the broadest peak ($\Delta T_{1/2}$ = 8.75 K) and the highest phase transition temperature (T_c = 32.47°C) (see Table 1). (The melting transition temperature given here is the temperature at the peak; both the peak and the onset temperatures of the transition are given in Table 1.) (*R*)-ET-18-OMe showed the lowest phase transition temperature and smallest full width at half maximum of the phase transition. However, (*R*)-Lyso-PAF gave the smallest enthalpy change (ΔH = 7.039 kcal/mol) and (*R*)-PAF the largest (ΔH = 7.912 kcal/mol). The DSC results confirm that the compounds were in the gel phase at 14°C, the temperature at which the X-ray diffraction experiments were conducted, and are consistent with the observed changes in *d*-spacing with temperature (Fig.

Table 1
Transition properties of the ether lipid analogs at 98% RH

Molecule	Phase transition onset (°C)	Phase transition peak (T_c) (°C)	FWHM [a] $\Delta T_{1/2}$ (K)	Enthalpy change ΔH (kcal/mol)
(*R*)-PAF	23.61	29.02	6.38	7.812
(*R*)-ET-18-OMe	23.70	28.50	6.00	7.910
(*R*)-Lyso-PAF	24.44	32.47	8.75	7.309

[a] Full width at half maximum.

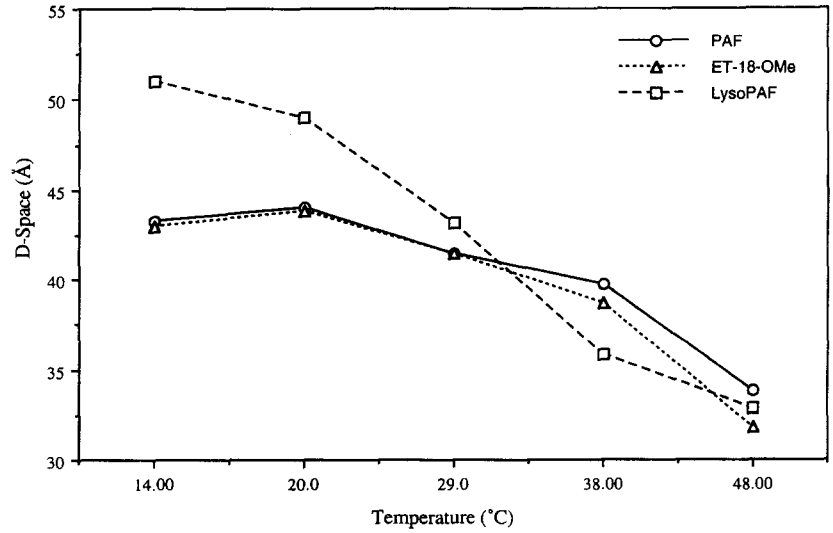

Fig. 6. Temperature dependence of *d*-spacing at 98% RH. Circles and solid line, (*R*)-PAF; triangles and dotted line, (*R*)-ET-18-OMe; squares and dashed line, (*R*)-Lyso-PAF. Each line shows the change in *d*-spacing of a single sample as it was heated, indicating the similar responses of the three compounds to warming. In each case the *d*-spacing decreased rapidly after the onset of the phase transition. (*R*)-Lyso-PAF shows the largest change in *d*-spacing.

6); that is, as the temperature rises, the *d*-spacing begins to decrease rapidly only after the phase transition has begun.

4. Discussion

The diffraction patterns and electron density profiles (Fig. 4) from (*R*)-PAF, (*R*)-ET-18-OMe and (*R*)-Lyso-PAF at 98% RH strongly indicate that the hydrocarbon chains of these ether lipids are interdigitated. The profiles in Fig. 4 are similar to those derived by Ranck et al. [29] for the interdigitated phase of dipalmitoylphosphatidylglycerol (DPPG) in the gel state. The electron density profiles show that the distances between headgroup peaks are 32.1, 30.6 and 35.6 Å for (*R*)-PAF, (*R*)-ET-18-OMe and (*R*)-Lyso-PAF, respectively, in contrast to the 43.8 Å expected for two fully extended DPPC chains that are not interdigitated in the gel phase at the same temperature. Moreover, the electron density profiles in Fig. 4 do not have the deep terminal methyl trough in the center of the profile that is observed when the hydrocarbon chains are not interdigitated and the methyl groups are localized in the bilayer center, as in noninterdigitated DPPC bilayers. Taking into account that the acyl chains of DPPC are 16 carbons long and those of the ether lipids are 18 carbons long, and assuming 1.25 Å/CH_2, the differences between the calculated bilayer width for fully extended non-interdigitating chains (48.8 Å) and the actual ether lipid bilayer widths for the interdigitating chains are 16.7 Å (13 CH_2), 18.2 Å (15 CH_2) and 13.2 Å (11 CH_2), for (*R*)-PAF, (*R*)-ET-18-OMe, and (*R*)-Lyso-PAF, respectively. According to this calculation, the hydrocarbon chains of these molecules have penetrated up to the 13th to 11th CH_2 group of the ether lipids of the opposing monolayer. However, these calculated differences are larger than the lengths of the interdigitated regions observed in the electron density profiles [(*R*)-PAF: 9.3 Å (7 CH_2), (*R*)-ET-18-OMe: 12.3 Å (10 CH_2) and (*R*)-Lyso-PAF: 6.8 Å (5 CH_2)]. Our explanation is that the chains may possibly be tilted in these interdigitated bilayers in the gel phase.

Computer graphical representations of bilayer structures that might explain the X-ray diffraction results were constructed. When the headgroup separation of (*R*)-ET-18-OMe was set at 41.5 Å, making the interdigitated portion of the chain 15.2 Å long, a tilt angle of 35° with respect to the bilayer normal yielded a headgroup-headgroup separation of 30.6 Å. The projection of the interdigitated portion of the chain on the bilayer normal was 11.9 Å, which is close to the experimental value (12.3 Å). A similar process applied to (*R*)-Lyso-PAF achieved vertical projections on the bilayer normal of 35.8 Å for the headgroup-headgroup distance and 7.7 Å for the interdigitated region. Other combinations of degree of interdigitation and tilt angle may also be consistent with the X-ray data.

These packing models of the ether lipid bilayers indicated that there may be some space (5–10 Å) between the terminal methyl groups of the chains and the glycerol backbone region of the opposing monolayer with which the chains are interdigitating. That space should allow the alkyl chains to penetrate farther into the opposite monolayer than the models indicate – the chains should interdigitate until the terminal methyl of the chains reaches the carbonyl of (*R*)-PAF, or ether oxygen of the (*R*)-ET-18-OMe, or -OH group of (*R*)-Lyso-PAF. However, the experimental data indicate that partial interdigitation of the alkyl chains is more likely than full interdigitation. The crystal structure of (*R*)-ET-18-OMe may provide an explanation of the difference [27]. In the crystal structure, further interdigitation is prevented by a molecule of water of hydration at the headgroup that is positioned in the path of the intruding hydrocarbon chains. The degree of water penetration into the bilayer depends on the composition of the lipid [30]. The substituent group at the 2-position of the glycerol backbone, especially the -OH group of (*R*)-Lyso-PAF, may hydrogen bond with water to expand the interface region and/or make it more polar. This expansion may prevent the chains from penetrating further, resulting in partial instead of full interdigitation. The observation that (*R*)-Lyso-PAF has the widest headgroup region also supports this explanation. The width of the headgroup region may also be modified by possible interactions between the charged regions of the headgroup and the substituent at the *sn*-2 position. Such interactions might affect headgroup orientation, and coupled with the high degree of hydration might alter the surface charge characteristics and the dielectric constant of the headgroup region relative to those of the other two ether lipids.

The DSC results are summarized in the Table. The calorimetric behavior of (*R*)-Lyso-PAF (broadest $\Delta T_{1/2}$, highest T_c and smallest ΔH) upon interdigitation can be rationalized as follows. The phase transition temperature is markedly dependent on the chain length and the chemical structure of the lipid hydrocarbon chains, as well as on the nature of the polar headgroup interactions [31,32]. All three molecules have the same *sn*-1 chains and the same phosphocholine headgroup. The only differences among the three occur at the glycerol backbone at the *sn*-2 chain, in the interface region. Therefore, the changes in $\Delta T_{1/2}$, T_c and ΔH are determined by the identity of the substituent group at the 2-position of glycerol backbone. At neutral pH all three molecules are zwitterions, but (*R*)-Lyso-PAF melts about 4 K higher than others. This reflects the ability of (*R*)-Lyso-PAF to interact with an adjacent (*R*)-Lyso-PAF molecule via hydrogen bonding, achieving higher stability. Because of its H-bonding, one might surmise that (*R*)-Lyso-PAF would have highest ΔH of the three, also. Actually, it has the smallest ΔH, which might be explained as follows. The X-ray data indicated different degrees of interdigitation in bilayers of the three molecules because of the structural differences at the 2-position of glycerol backbone. (*R*)-ET-18-OMe and (*R*)-PAF are interdigitated farther than (*R*)-Lyso-PAF. The interdigitated

parts of the alkyl chains would restrict one another and adopt an almost all-*trans* conformation to achieve minimum energy in the gel phase. (*R*)-Lyso-PAF has less extensively interdigitated alkyl chains, so the non-interdigitated part of the alkyl chain may adopt more *gauche* conformations, causing (*R*)-Lyso-PAF to have higher energy in the gel phase. Fourier transform infrared spectroscopy (FTIR) could be used to test this hypothesis. However, FTIR has shown that in DPPC in the liquid crystalline state, there are only about 3.6–4.2 *gauche* conformations per chain [33,34]. For these saturated ether lipids in the gel state, even fewer *gauche* conformations might be expected.

(*R*)-Lyso-PAF would also need less energy (ΔH) to overcome the energy barrier for melting. (*R*)-PAF and (*R*)-ET-18-OMe have lower energy in the gel phase and need more energy to pass the barrier, so their enthalpy changes (ΔH) are larger than that of (*R*)-Lyso-PAF. We have assumed that the contribution of H-bonding to ΔH is smaller than that of interdigitation. The wide melting temperature range and broad endotherm (largest $\Delta T_{1/2}$) of (*R*)-Lyso-PAF indicate that its cooperativity is poor; the packing properties indicated by the diffraction data are consistent with this idea.

The phase behavior of 1-*O*-octadecyl-2-*O*-methyl-*rac*-glycero-3-phosphocholine has been investigated in the temperature range −10 to 40°C by Maurer et al., using dispersions of micelles prepared at 40°C [35]. (Our vesicle samples probably also contain some micelles in addition to multilamellar vesicles.) Lipid dispersions exhibited endotherms at 2.5, 17, and 20°C on heating, but only one transition, from a micellar to a lamellar gel phase at 6°C, during recooling. Below 6°C X-ray diffraction indicated a lamellar phase ($d = 51$ Å) with tilted and/or interdigitated chains. Huang et al. have used Raman and ^{31}P-NMR spectroscopy to study the phase transitions of PAF in aqueous dispersions [36]. Two transitions were observed, at 9.2°C (large vesicles of interdigitated lamellar gel to smaller vesicles of more disordered interdigitated lamellar gel) and 18.4°C (interdigitated lamellar gel to micellar phase). Our X-ray diffraction results also indicate an interdigitated lamellar phase for these compounds at 98% RH. Our DSC results show different transition temperatures, because of the lower hydration state and oriented multilayer form of our samples.

5. Conclusions

The amphipathic ether lipids discussed here appear to form bilayers similar to lipid bilayers, with interdigitated and probably tilted chains. The results indicate that these molecules might easily insert themselves into membrane bilayers and align themselves in the bilayer like natural lipids. Biological membranes are a site of drug action. Drugs must get into or pass through membranous barriers to reach their receptors (if they exist), or perturb membranes and modify the properties of the bilayer or those of the membrane-associated functional proteins. Perturbation of the membrane may be related to the recently reported anti-HIV activity of (*R*)-ET-18-OMe. The very low biological activity of (*R*)-Lyso-PAF may be due to its higher capacity for hydration and hydrogen bonding.

The ether lipids represent a new class of biologically active agents whose pharmacology is not yet understood and which are attracting considerable attention. Presently, we are carrying out high-resolution 2D-NMR experiments combined with computer simulation to study the conformation of these molecules.

Acknowledgements

This project was supported by the grants from Glaxo and the University of Connecticut Research Foundation. The X-ray diffraction experiments were carried out in the Biomolecular Structure Analysis Center at the University of Connecticut Health Center (directed by Dr. Leo G. Herbette). The authors would like to thank Dr. David G. Rhodes, Dr. R. Preston Mason, Dr. Mark W. Trumbore, Dr. David W. Chester, and Dr. Richard I. Duclos, Jr., for helpful discussions.

References

[1] Munder, P.G., Modolell, M., Andreesen, R., Weltzien, H.U. and Westphal, O. (1979) Springer Semin. Immunopathol. 2, 187–203.
[2] Weltzien, H.U. and Munder, P.G. (1983) in Etherlipids (Mangold, H.K. and Paltauf, F., eds.), Academic Press, New York.
[3] Eibl, H. (1984) Angew. Chem. 96, 247–262.
[4] Eibl, H. (1984) Angew. Chem. Int. Edn. 23, 257–271.
[5] Berdel, W.E. (1987) Lipids 22, 970–973.
[6] Stewart, A.G. (1994) in Lipid Mediators (Cunningham, F.M., eds.), pp. 221–295, Academic Press, New York.
[7] Chao, W. and Olson, M.S. (1993) Biochem. J. 292, 617–629.
[8] Imaizumi, T.-A., Stafforini, D.M., Yamada, Y., McIntire, T.M., Prescott, S.M. and Zimmerman, G.A. (1995) J. Intern. Med. 238, 5–20.
[9] Pinckard, R.N., Woodard, D.S., Showell, H.J., Conklyn, M.J., Novak, M.J. and McManus, L.M. (1995) Clin. Rev. Allergy 12, 329–359.
[10] Pinckard, R.N., McManus, L.M. and Hanahan, D.J. (1982) Adv. Inflammation Res. 4, 147–180.
[11] Berdel, W.E., Greiner, E., Fink, U., Zanker, K.S., Stavrou, D., Trappe, A., Fahlbush, R., Reichert, A. and Rastetter, J. (1984) Oncology 41, 140–145.
[12] Duclos, R.I., Chia, H.H., Abdelmageed, O.H., Esber, H., Fournier, D.J. and Makriyannis, A. (1994) J. Med. Chem. 37, 4147–4154.
[13] Kucera, L.S., Iyer, N., Leake, E., Raben, A., Modest, E.J., Daniel, L.W. and Piantadosi, C. (1990) Aids Res. Hum. Retrovirus 6, 6491–501.
[14] Lin, H.-N., Wang, Z.-Q. and Huang, C.-H. (1991) Biochim. Biophys. Acta 1067, 17–28.
[15] Xu, H., Stephenson, F.A. and Huang, C.-H. (1987) Biochemistry 26, 5448–5453.
[16] Hirth, B. and Barner, R. (1982) Helv. Chim. Acta 65, 1059–1084.

[17] Berchtold, R. (1982) Chem. Phys. Lipids 30, 389–392.
[18] Takano, S., Akiyama, M. and Ogasawara, K. (1984) Chem. Pharm. Bull. 32, 791–794.
[19] Hirt, R. and Berchtold, R. (1958) Pharm. Acta Helv. 33, 349–356.
[20] Eibl, H. and Nicksch, A. (1978) Chem. Phys. Lipids 22, 1–8.
[21] Hansen, W.J., Murari, R., Wedmid, Y. and Baumann, W.J. (1982) Lipids 17, 453–459.
[22] Godfroid, J.J., Heymand, F., Michel, E., Redeuilh, C., Steinen, E. and Benveniste, J. (1980) FEBS Lett. 116, 161–164.
[23] Abdelmageed, O.H., Duclos, R.I., Jr., Abushanab, E. and Makriyannis, A. (1994) Chem. Phys. Lipids 54, 49–59
[24] Dale, J.A., Dull, D.L. and Mosher, H.S. (1969) J. Org. Chem. 34, 2543–2549.
[25] Bourges, M., Small, D.M. and Dervichian, D.G. (1967) Biochim. Biophys. Acta 137, 157–167.
[26] Franks, N.P. (1976) J. Mol. Biol. 100, 345–358.
[27] Pascher, I., Sundell, S., Eibl, H. and Harlos, K. (1986) Chem. Phys. Lipids 39, 53–64.
[28] Perutz, M.F. (1954) Proc. Roy. Soc. Ser. A, 225, 264–286.
[29] Ranck, J.L., Keira, T. and Luzzati, V. (1977) Biochim. Biophys. Acta 488, 432–441.
[30] Simon, S.A., McIntosh, T.J. and Latorre, R. (1982) Science 216, 65–67.
[31] Melchior, D.L. and Steim, J.M. (1976) Annu. Rev. Biophys. Bioeng. 5, 205–238.
[32] McElhaney, R.N. (1982) Chem. Phys. Lipids 30, 229–259.
[33] Casal, H.L. and McElhaney, R.N. (1990) Biochemistry 29, 5423–5427.
[34] Mendelsohn, R., Davies, M.A., Brauner, J.W., Schuster, H.F. and Dluhy, R.A. (1989) Biochemistry 28, 8934–8939.
[35] Maurer, N., Prenner, E., Paltauf, R. and Glatter, O. (1994) Biochim. Biophys. Acta 1192, 167–176.
[36] Huang, C., Mason, J.T., Stephenson, F.A. and Levin, I.W. (1986) Biophys. J. 49, 587–595.